





Terahertz spin-orbit torque as a drive of spin dynamics in insulating antiferromagnet Cr_2O_3

R. M. Dubrovin ^{1,*} Z. V. Gareeva ^{2,3} A. V. Kimel ⁴ and A. K. Zvezdin ^{5,6,†}

¹*Ioffe Institute, Russian Academy of Sciences, 194021 St. Petersburg, Russia*

²*Institute of Molecule and Crystal Physics, Ufa Federal Research Center, Russian Academy of Sciences, 450075 Ufa, Russia*

³*Ufa University of Science and Technology, 450076 Ufa, Russia*

⁴*Institute for Molecules and Materials, Radboud University, 6525 AJ Nijmegen, The Netherlands*

⁵*New Spintronic Technologies LLC, 121205 Skolkovo, Moscow, Russia*

⁶*Prokhorov General Physics Institute, Russian Academy of Sciences, 119991 Moscow, Russia*

(Dated: August 1, 2025)

Contrary to conventional wisdom that spin dynamics induced by current are exclusive to metallic magnets, we theoretically predict that such phenomena can also be realized in magnetic insulators, specifically in the magnetoelectric antiferromagnet Cr_2O_3 . We reveal that the displacement current driven by the THz electric field is able to generate a Néel spin-orbit torque in this insulating system. By introducing an alternative electric dipole order parameter arising from the dipole moment at Cr^{3+} sites, we combine symmetry analysis with a Lagrangian approach and uncover that the displacement current couples to the antiferromagnetic spins and enables ultrafast control of antiferromagnetic order. The derived equations of motion show that this effect competes with the linear magnetoelectric response, offering a novel pathway for manipulating antiferromagnetic order in insulators. Our findings establish insulator antiferromagnets as a viable platform for electric field driven antiferromagnetic spintronics and provide general design principles for non-metallic spin-orbit torque materials.

INTRODUCTION

After three decades of successful development, ferromagnetic spintronics starts facing fundamental challenges [1], which can no longer be resolved by marginal improvements and require a paradigm shift. Antiferromagnetic spintronics is seen as one of the most promising routes for further developments. Simultaneously, antiferromagnetic spintronics is also a challenge, as antiferromagnets often have no net magnetization and are weakly sensitive to external magnetic fields. Finding the most efficient ways to control spins in antiferromagnets is already for many decades a topic of research [2–5]. The ability to generate strong and nearly single cycle THz pulses of electromagnetic radiation has managed to become a game changer in the field. Using the pulses, it was demonstrated that spin dynamics in antiferromagnets with no net magnetization can be launched by both THz magnetic [6–9] and electric fields [10]. THz electric current is also able to drive spin dynamics in metallic antiferromagnets, e.g., Mn_2Au and CuMnAs , through the Néel spin-orbit torque [11–20]. The origin of this torque is the Rashba–Edelstein effect, in which an electric current leads to spin polarization with different signs on different antiferromagnetic sublattices. A similar mechanism was anticipated for Cr_2O_3 at doping into the semiconducting or metallic regime [21].

Here, we present a theoretical study of the so far overlooked effect of THz electric field on antiferromag-

netic spins. The effect is similar to the Néel spin orbit torque, while originating from displacement currents and thus quite possible in materials with a electric poor conductivity, such as Cr_2O_3 . Using this prototypical insulating magnetoelectric antiferromagnet, we theoretically demonstrate that even in the absence of conduction electrons when Ohm’s currents can be neglected, a control of antiferromagnetic spins is possible via coupling the antiferromagnetic order parameter to the displacement current induced by the terahertz electric field. We have considered the crystal structure of Cr_2O_3 within the point charge model and found electric dipole moments ordered antiparallel along the antiferromagnetic ordering axis on the sites of Cr^{3+} magnetic ions. Furthermore, we have shown that from symmetry it is necessary to include the electric dipole order parameter in this coupling. Employing a Lagrangian approach, we derived the equations of spin dynamics in which the spin-orbit torque and the linear magnetoelectric effect enter in a similar way. Thus, in addition to the earlier reported mechanisms to control spins in antiferromagnets using magnetic field, electric field or electric current, here we demonstrate the control using displacement currents similar to the Néel spin orbit torque. The mechanism is expected to be especially strong in insulating antiferromagnets, where the conventional Néel spin orbit torque has been neglected so far.

RESULTS

Cr_2O_3 with corundum structure (space group $R\bar{3}c$, $Z = 2$) is the prototypical linear magnetoelectric antiferromagnet [22–25]. Below the Néel temperature $T_N =$

* dubrovin@mail.ioffe.ru

† zvezdin.ak@phystech.edu

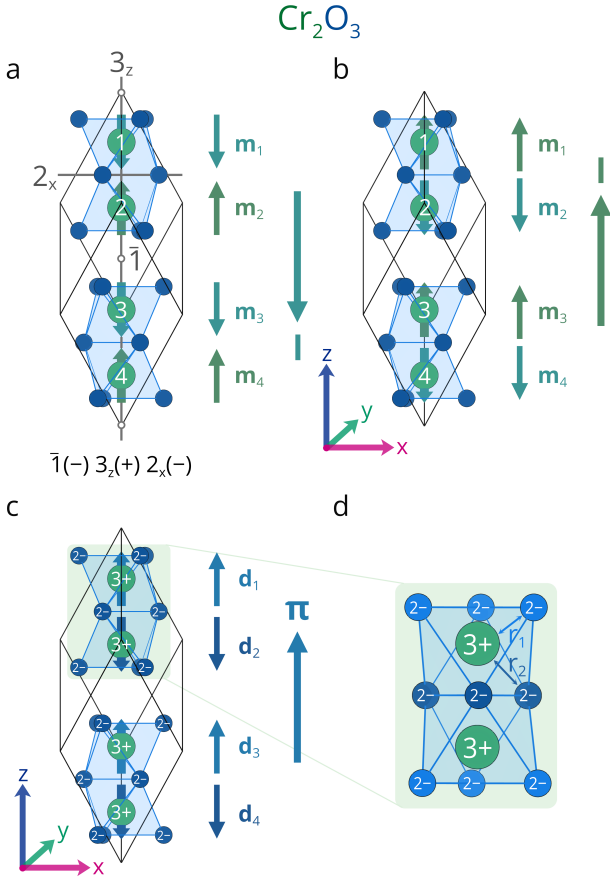


FIG. 1. **Crystal, magnetic and electric dipole structures of antiferromagnet Cr_2O_3 .** Unit cell with antiferromagnetic vectors \mathbf{l}_\downarrow (a) and \mathbf{l}_\uparrow (b). Green arrows denote the orientation of magnetic moments \mathbf{m}_1 – \mathbf{m}_4 of Cr^{3+} ions (labelled 1–4). Positions of the symmetry elements $\bar{1}$, 3_z , and 2_x in the unit cells are given in panel (a). (c) Electric dipole moments \mathbf{d}_1 – \mathbf{d}_4 (blue arrows) in the unit cell in the vicinity of magnetic Cr^{3+} ions. The nominal charges of Cr^{3+} and O^{2-} ions in e are given. (d) The nearest O^{2-} cations are located at two different distances r_1 and r_2 from the Cr^{3+} ions as marked in light and dark blue.

307 K [26, 27], the magnetic moments of Cr^{3+} of the same value of magnetizations $|\mathbf{m}_1| = |\mathbf{m}_2| = |\mathbf{m}_3| = |\mathbf{m}_4| = m_0$ are antiferromagnetically ordered along the 3_z axis, resulting in one of two types of antiferromagnetic ordering [28–30], as shown in Figs. 1(a) for $\downarrow\uparrow\downarrow\uparrow$ and 1(b) for $\uparrow\downarrow\uparrow\downarrow$. It is convenient to use the double-sublattice approximation in which co-directional magnetizations are replaced by two normalized magnetizations $\mathbf{m}_A = \frac{\mathbf{m}_1 + \mathbf{m}_3}{2m_0}$ and $\mathbf{m}_B = \frac{\mathbf{m}_2 + \mathbf{m}_4}{2m_0}$. This allows us to introduce the net magnetization vector $\mathbf{m} = \frac{\mathbf{m}_A + \mathbf{m}_B}{2}$ and antiferromagnetic Néel vector $\mathbf{l} = \frac{\mathbf{m}_A - \mathbf{m}_B}{2}$. Further, we will use the Cartesian coordinate system in which $z \parallel \mathbf{l}$ as shown in Fig. 1.

TABLE I. Permutation transformations of Cr^{3+} ions 1–4, magnetic \mathbf{m} , \mathbf{l}_1 – \mathbf{l}_3 and electric \mathbf{p} , $\boldsymbol{\pi}_1$ – $\boldsymbol{\pi}_3$ basis vectors under the action of generators $\bar{1}$, 3_z , and 2_x of the groups for Cr_2O_3 .

	1	2	3	4	\mathbf{m}	\mathbf{l}_1	\mathbf{l}_2	\mathbf{l}_3	\mathbf{p}	$\boldsymbol{\pi}_1$	$\boldsymbol{\pi}_2$	$\boldsymbol{\pi}_3$
$\bar{1}$	4	3	2	1	\mathbf{m}	\mathbf{l}_1	$-\mathbf{l}_2$	$-\mathbf{l}_3$	$-\mathbf{p}$	$-\boldsymbol{\pi}_1$	$\boldsymbol{\pi}_2$	$\boldsymbol{\pi}_3$
3_z	1	2	3	4	\mathbf{m}	\mathbf{l}_1	\mathbf{l}_2	\mathbf{l}_3	\mathbf{p}	$\boldsymbol{\pi}_1$	$\boldsymbol{\pi}_2$	$\boldsymbol{\pi}_3$
2_x	2	1	4	3	\mathbf{m}	$-\mathbf{l}_1$	$-\mathbf{l}_2$	\mathbf{l}_3	$-\mathbf{p}$	$\boldsymbol{\pi}_1$	$\boldsymbol{\pi}_2$	$-\boldsymbol{\pi}_3$

It is interesting to note that, if we attribute nominal charges to atomic cores, e.g. $+3e$ for Cr^{3+} and $-2e$ for O^{2-} , so that the electroneutrality of the Cr_2O_3 unit cell is preserved, in the simple point charge model [31–33], the non-zero dipole moments $\mathbf{d}_i = q_i \mathbf{r}$ oriented along the z axis appear in the vicinity of Cr^{3+} ions $i = 1$ –4, as shown in Fig 1(c). The dipole moments originate from the asymmetric arrangement of O^{2-} anions at two distinct distances r_1 and r_2 from the Cr^{3+} cation, as can be seen in detail in Fig. 1(d) where equidistant oxygens are represented by colour. We emphasize that, according to Refs. [34], the dipole moment can be represented as $\mathbf{d} = \mathbf{d}_{\text{ion}} + \mathbf{d}_{\text{el}}$, where the ionic contribution \mathbf{d}_{ion} is estimated by the point charge model, while the electronic term \mathbf{d}_{el} accounting for the covalent bonding between the atoms is calculated using the Berry-phase approach. In our consideration, we assume that Cr_2O_3 is a fully ionic crystal, and thus neglect the contribution from the dipole moment \mathbf{d}_{el} caused by electrons. As in the case of magnetic moments, these dipole moments have the same values $|\mathbf{d}_1| = |\mathbf{d}_2| = |\mathbf{d}_3| = |\mathbf{d}_4| = d_0$, and they are ordered in such a way that the total dipole moment of the unit cell is zero. Note that such ordering of dipole moments is close to that observed in antiferroelectrics [35, 36]. Next, by analogy with antiferromagnets, we will use the double-sublattice approximation and define two normalized dipole moments $\mathbf{d}_A = \frac{\mathbf{d}_1 + \mathbf{d}_3}{2d_0}$ and $\mathbf{d}_B = \frac{\mathbf{d}_2 + \mathbf{d}_4}{2d_0}$, and the net polarization $\mathbf{p} = \frac{\mathbf{d}_A + \mathbf{d}_B}{2}$ and antiferroelectric vector $\boldsymbol{\pi} = \frac{\mathbf{d}_A - \mathbf{d}_B}{2}$.

From a symmetry point of view, the trigonal space groups can be represented by three generators of the group (independent symmetry elements), which include an inversion center $\bar{1}$ ($x \rightarrow -x$, $y \rightarrow -y$, $z \rightarrow -z$), a three-fold axis $3_z \parallel z$ ($x \rightarrow -\frac{1}{2}[x - \sqrt{3}y]$, $y \rightarrow -\frac{1}{2}[\sqrt{3}x + y]$, $z \rightarrow z$) and a two-fold axis $2_x \parallel x$ ($x \rightarrow x$, $y \rightarrow -y$, $z \rightarrow -z$) [37]. The action of these symmetry elements can be illustrated, if we keep in mind that in the case of four magnetic ions in a unit cell of Cr_2O_3 we should define four magnetic and four electric basis

vectors by the following way:

$$\begin{aligned}\mathbf{m} &= \frac{\mathbf{m}_1 + \mathbf{m}_2 + \mathbf{m}_3 + \mathbf{m}_4}{4m_0}, \\ \mathbf{l}_1 &= \frac{\mathbf{m}_1 - \mathbf{m}_2 - \mathbf{m}_3 + \mathbf{m}_4}{4m_0}, \\ \mathbf{l}_2 &= \frac{\mathbf{m}_1 - \mathbf{m}_2 + \mathbf{m}_3 - \mathbf{m}_4}{4m_0}, \\ \mathbf{l}_3 &= \frac{\mathbf{m}_1 + \mathbf{m}_2 - \mathbf{m}_3 - \mathbf{m}_4}{4m_0},\end{aligned}\quad (1)$$

and

$$\begin{aligned}\mathbf{p} &= \frac{\mathbf{d}_1 + \mathbf{d}_2 + \mathbf{d}_3 + \mathbf{d}_4}{4d_0}, \\ \boldsymbol{\pi}_1 &= \frac{\mathbf{d}_1 - \mathbf{d}_2 - \mathbf{d}_3 + \mathbf{d}_4}{4d_0}, \\ \boldsymbol{\pi}_2 &= \frac{\mathbf{d}_1 - \mathbf{d}_2 + \mathbf{d}_3 - \mathbf{d}_4}{4d_0}, \\ \boldsymbol{\pi}_3 &= \frac{\mathbf{d}_1 + \mathbf{d}_2 - \mathbf{d}_3 - \mathbf{d}_4}{4d_0}.\end{aligned}\quad (2)$$

From Eqs. (1) and (2) we see that the antiferromagnetic and antiferroelectric vectors correspond to $\mathbf{l} = \mathbf{l}_2$ and $\boldsymbol{\pi} = \boldsymbol{\pi}_2$. The group generators perform permutations of magnetic ions which in turn lead to the transformation of magnetic and electric basis vectors as shown in Table I.

The generators of the group can be divided into two types based on their permutation properties with respect to the selected position of the magnetic ions. A symmetry element is labelled with an index (+) if it permutes ions to positions belonging to the same magnetic sublattice with equally oriented magnetizations, and with (−) if the resulting sublattice is opposite. According to these rules, we can write the symmetry elements adopted as the generators of the space groups $\bar{1}(-) 3_z(+) 2_x(-)$ for Cr_2O_3 , as can be seen in Fig. 1. From Table I, we see that $3_z(+)$ transforms \mathbf{m} and $\mathbf{l} = \mathbf{l}_2$ in the same way, whereas under the action of $\bar{1}(-)$ and $2_x(-)$ the vector $\mathbf{l} = \mathbf{l}_2$ changes sign. It is worth noting that in a similar way these indices relate polarization \mathbf{p} and antiferroelectric vector $\boldsymbol{\pi}$. Thus, the (+) and (−) indices are relevant only for antiferromagnetic \mathbf{l} and antiferroelectric $\boldsymbol{\pi} = \boldsymbol{\pi}_2$ vectors, which, under the action of a symmetry element, are transformed like axial and polar vectors multiplied by the sign of the index, respectively. For example, $\bar{1}(-) \mathbf{m} = \mathbf{m}$ and $\bar{1}(-) \mathbf{p} = -\mathbf{p}$, whereas $\bar{1}(-) \mathbf{l} = -\mathbf{l}$ and $\bar{1}(-) \boldsymbol{\pi} = \boldsymbol{\pi}$. Note that in our case the magnetic sublattices coincide with electric dipole sublattices (see Fig. 1), but if these sublattices do not match then the indices can be different, e.g. $\bar{1}(-)$ for magnetic and $\bar{1}(+)$ for electric basis vectors. Thus, the set of generators, written in this way, and called an exchange magnetic structure, provides all the necessary information to find the invariant form of a thermodynamic potential or a material tensor in terms of magnetization \mathbf{m} , antiferromagnetic vector \mathbf{l} , polarization \mathbf{p} , antiferroelectric vector $\boldsymbol{\pi}$, electric current \mathbf{j} , etc., for antiferromagnets as detailed in Refs. [37, 38].

TABLE II. Transformation of the magnetization \mathbf{m} , antiferromagnetic vector \mathbf{l} , electric current \mathbf{j} , polarization \mathbf{p} and antiferroelectric vector $\boldsymbol{\pi}$ under the action of symmetry elements $\bar{1}(-)$, $3_z(+)$, $2_x(-)$.

Dynamical variable	$\bar{1}(-)$	$3_z(+)$	$2_x(-)$
m_x	m_x	$-(m_x - \sqrt{3}m_y)/2$	m_x
m_y	m_y	$-(\sqrt{3}m_x + m_y)/2$	$-m_y$
m_z	m_z	m_z	$-m_z$
l_x	$-l_x$	$-(l_x - \sqrt{3}l_y)/2$	$-l_x$
l_y	$-l_y$	$-(\sqrt{3}l_x + l_y)/2$	$-l_y$
l_z	$-l_z$	l_z	l_z
j_x	$-j_x$	$-(j_x - \sqrt{3}j_y)/2$	j_x
j_y	$-j_y$	$-(\sqrt{3}j_x + j_y)/2$	$-j_y$
j_z	$-j_z$	j_z	$-j_z$
p_x	$-p_x$	$-(p_x - \sqrt{3}p_y)/2$	p_x
p_y	$-p_y$	$-(\sqrt{3}p_x + p_y)/2$	$-p_y$
p_z	$-p_z$	p_z	$-p_z$
π_x	π_x	$-(\pi_x - \sqrt{3}\pi_y)/2$	$-\pi_x$
π_y	π_y	$-(\sqrt{3}\pi_x + \pi_y)/2$	π_y
π_z	π_z	π_z	π_z

From Table II we see that the combination of components of the antiferromagnetic vector and electric current $l_x j_y - l_y j_x$ is invariant with respect to the action of symmetry elements for $\bar{1}(-) 3_z(+) 2_x(-)$ in Cr_2O_3 . It is noteworthy that this represents the z component of the cross product of the antiferromagnetic vector \mathbf{l} and the electric current \mathbf{j} , given by $[\mathbf{l} \times \mathbf{j}]_z = l_x j_y - l_y j_x$. It is interesting to emphasize that this invariant is similar to one $\sigma_x k_y - \sigma_y k_x$ included in the Rashba hamiltonian [39–42], where $\boldsymbol{\sigma}$ and \mathbf{k} are the carrier's spin angular and linear momentum, respectively, and $l_x m_y - l_y m_x$ underlies the Dzyaloshinskii-Moriya interaction [37]. For the term $[\mathbf{l} \times \mathbf{m}]_z = l_x m_y - l_y m_x$ to be invariant, it is required that $\bar{1}(+)$ which leads to \mathbf{l} being an axial vector that does not change sign under the space inversion $\bar{1}$. Then the free energy related to the Dzyaloshinskii-Moriya interaction can be represented as follows [43]

$$\mathcal{F}_D \simeq d [\mathbf{l} \times \mathbf{m}], \quad (3)$$

where $d \parallel z$ is the t -even Dzyaloshinskii axial vector. In turn, the existence of the linear magnetoelectric effect requires that $\bar{1}(-)$ which in turn leads to \mathbf{l} being an axial vector that changes sign under the space inversion $\bar{1}$. In this case, the free energy related to the interaction of electric current \mathbf{j} with the antiferromagnetic vector \mathbf{l} can be written as follows

$$\mathcal{F}_{\text{SOT}} \simeq \boldsymbol{\pi} [\mathbf{l} \times \mathbf{j}], \quad (4)$$

where $\boldsymbol{\pi} \parallel z$ is the t -even antiferroelectric polar vector that does not change sign under the space inversion $\bar{1}$. It is interesting to note that the SOT driven magnetic dynamics in symmetry forbidden in the

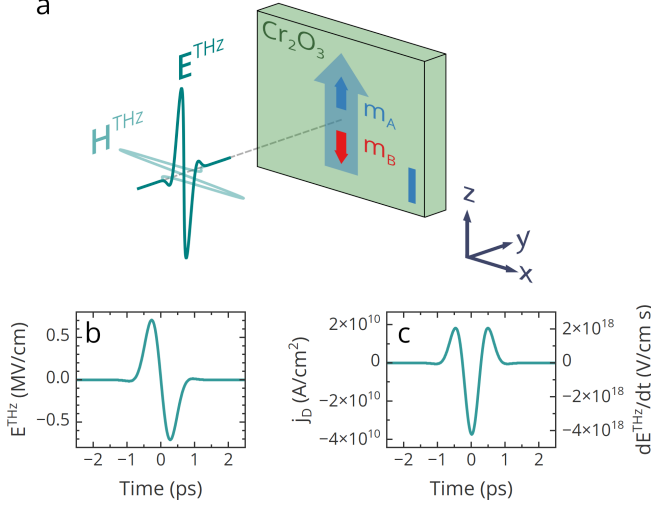


FIG. 2. **Schematic of the THz experiment.** (a) Geometry of the considered experiment, in which dynamics of the antiferromagnetic vector $\mathbf{l} = \mathbf{m}_A - \mathbf{m}_B$ in Cr₂O₃ is driven by a THz nearly single cycle pulse. Time traces of (b) the THz electric field \mathbf{E}^{THz} and (c) the resulting displacement current $\mathbf{j}_D \propto \dot{\mathbf{E}}$ along with the time derivative $\dot{\mathbf{E}}$.

isostructural antiferromagnet hematite $\alpha\text{-Fe}_2\text{O}_3$ with different spin ordering and the exchange magnetic structure $\bar{1}(+)3_z(+)2_x(-)$ which eliminates the invariant $\pi_z (l_x j_y - l_y j_x)$.

It is worth noting that this kind of coupling between the electric current \mathbf{j} and antiferromagnetic vector \mathbf{l} is well known in metallic antiferromagnets such as Mn₂Au and CuMnAs and it is related to Néel spin-orbit torque [11–20]. It is clear that, since Cr₂O₃ single crystal is a good insulator, the electric currents flowing through it are negligible. However, according to Maxwell's equations, there is a displacement current in insulators which is caused by the motion of bound charges and, according to Maxwell's equations, like electric current, results in a magnetic field [44–46]. The displacement current in

the Gaussian system of units has the form $\mathbf{j}_D = \frac{\epsilon}{4\pi} \dot{\mathbf{E}}$, where ϵ is the dielectric permittivity. We anticipate that the dielectric permittivity in the relevant frequency range will exhibit negligible deviation from the static dielectric permittivity. The latter is described by a diagonal tensor with two independent components, $\epsilon_x = 10.33$ and $\epsilon_z = 11.93$ [47], the difference between which we disregard for simplicity. We consider an experiment with a near single-cycle THz pulse with a duration of about 2 ps, spectral maximum at 0.6 THz and a peak electric field strength of 760 kV/cm as shown in Figs. 2(a) and 2(b). The time derivative reveals the displacement current $\mathbf{j} \propto \dot{\mathbf{E}}^{\text{THz}}$ induced in Cr₂O₃ by this THz pulse with a peak amplitude about 4×10^{10} A/cm² as shown in Fig. 2(c). Next, we can evaluate the effective conductivity $\mathbf{j}_D = \sigma_{\text{eff}} \mathbf{E}^{\text{THz}}$, which takes the values about $\sigma_{\text{eff}} \simeq 5.3 \times 10^6$ S/m $\simeq 4.8 \times 10^{16}$ s⁻¹, which is close to

the conductivity value in metallic antiferromagnets [18]. Thus, it is interesting to explore how the displacement current \mathbf{j}_D induced by the THz electric field \mathbf{E}^{THz} drives the dynamics of the antiferromagnetic vector \mathbf{l} through spin-orbit torque (SOT) in the magnetoelectric Cr₂O₃.

To reveal the key differences between the linear magnetoelectric effect and SOT, we develop a model of spin dynamics driven by the THz pulses in Cr₂O₃ with the antiferromagnetic vector $\mathbf{l} \parallel z$ using a non-standard spherical coordinate system where the polar angle ϑ counts from the y axis and the azimuthal angle φ lies in the xz plane and counts from the x axis. First, we need to define expressions for the energy of the spin system of Cr₂O₃ near the ground state using Eq. (32) from Methods section. The kinetic energy of a double-sublattice antiferromagnet in the first order in ϵ and β can be represented as [48, 49]

$$T = \frac{m_0}{\gamma} (\epsilon \dot{\varphi}_1 + \beta \dot{\vartheta}_1), \quad (5)$$

where γ is the gyromagnetic ratio. The exchange energy taking into account Eq. (29) has the next form in the second order of ϵ and β up to a constant term

$$U_{\text{Ex}} = \lambda_{\text{Ex}} m_0^2 \mathbf{m}_A \cdot \mathbf{m}_B \approx 2 \lambda_{\text{Ex}} m_0^2 (\epsilon^2 + \beta^2), \quad (6)$$

where $\lambda_{\text{Ex}} = 1/\chi_{\perp}$ is the exchange interaction between neighbouring spins of Cr³⁺ ions and χ_{\perp} is the perpendicular magnetic susceptibility. The energy of the uniaxial magnetic anisotropy in the second order in φ_1 and ϑ_1 up to a constant term is

$$U_A = -K l_z^2 \approx K (\varphi_1^2 + \vartheta_1^2), \quad (7)$$

where K is the uniaxial anisotropy constant.

The Zeeman interaction of the antiferromagnet with the external magnetic field \mathbf{H} , taking into account Eq. (32), has the following form

$$U_Z = -m_0 \mathbf{m} \cdot \mathbf{H} = -m_0 [m_x H_x + m_y H_y + m_z H_z] \approx -m_0 [\mp \beta H_x + \epsilon H_y \pm (\epsilon \vartheta_1 - \beta \varphi_1) H_z]. \quad (8)$$

According to Ref. [37], the general expression for the linear magnetoelectric interaction energy in Cr₂O₃ in the second order in small angles is

$$\begin{aligned} U_{\text{ME}} = & -\lambda_{\text{ME1}} m_0 [(l_x m_y + l_y m_x) E_x + (l_x m_x - l_y m_y) E_y] \\ & -\lambda_{\text{ME2}} m_0 m_z (l_x E_x + l_y E_y) - \lambda_{\text{ME3}} m_0 l_z (m_x E_x + m_y E_y) \\ & -\lambda_{\text{ME4}} m_0 (l_x m_x + l_y m_y) E_z - \lambda_{\text{ME5}} m_0 l_z m_z E_z \\ \approx & -\lambda_{\text{ME1}} m_0 [\pm (\beta \vartheta_1 - \epsilon \varphi_1) E_x + (\beta \varphi_1 + \epsilon \varphi_1) E_y] \\ & -\lambda_{\text{ME3}} m_0 (-\beta E_x \pm \epsilon E_y) - \lambda_{\text{ME4}} m_0 (\beta \varphi_1 - \epsilon \vartheta_1) E_z \\ & -\lambda_{\text{ME5}} m_0 (\epsilon \vartheta_1 - \beta \varphi_1) E_z, \end{aligned} \quad (9)$$

where $\lambda_{\text{ME1-5}}$ are magnetoelectric parameters. Strictly speaking, the electric polarization \mathbf{P} should be written instead of electric field \mathbf{E} in this expression, since \mathbf{P} is a dynamical variable of the medium. But for insulating

crystals, the polarization response to an electric field is given by the linear relation $\mathbf{P} = \frac{\varepsilon - 1}{4\pi} \mathbf{E}$.

Finally, the SOT interaction energy is

$$\begin{aligned} U_{\text{SOT}} &= -\lambda_{\text{SOT}} m_0 \pi_z (l_x j_y - l_y j_x) \\ &\approx -\lambda_{\text{SOT}} m_0 \pi_z \varepsilon / (4\pi) (\mp \varphi_1 \dot{E}_y + \vartheta_1 \dot{E}_x), \end{aligned} \quad (10)$$

where λ_{SOT} is the SOT parameter.

To describe the spin dynamics in Cr_2O_3 we employ a Lagrangian using Eqs. (5), (6), (7), (8), (10) and (9)

$$\begin{aligned} \mathcal{L} &= T - U_{\text{Ex}} - U_{\text{A}} - U_{\text{Z}} - U_{\text{SOT}} - U_{\text{ME}} \\ &= \frac{m_0}{\gamma} (\epsilon \dot{\varphi}_1 + \beta \dot{\vartheta}_1) - 2\lambda_{\text{Ex}} m_0^2 (\epsilon^2 + \beta^2) - K (\varphi_1^2 + \vartheta_1^2) \\ &\quad + m_0 [\mp \beta H_x + \epsilon H_y \pm (\epsilon \vartheta_1 - \beta \varphi_1) H_z] \\ &\quad + \lambda_{\text{ME1}} m_0 [\pm (\beta \vartheta_1 - \epsilon \varphi_1) E_x + (\beta \varphi_1 + \epsilon \vartheta_1) E_y] \\ &\quad + \lambda_{\text{ME3}} m_0 (-\beta E_x \pm \epsilon E_y) + \lambda_{\text{ME4}} m_0 (\beta \varphi_1 - \epsilon \vartheta_1) E_z \\ &\quad + \lambda_{\text{ME5}} m_0 (\epsilon \vartheta_1 - \beta \varphi_1) E_z \\ &\quad + \lambda_{\text{SOT}} m_0 \pi_z \varepsilon / (4\pi) (\mp \varphi_1 \dot{E}_y + \vartheta_1 \dot{E}_x). \end{aligned} \quad (11)$$

Then using the Lagrangian (11), we solve the Euler-Lagrange equations

$$\frac{d}{dt} \frac{\partial \mathcal{L}}{\partial \dot{q}_i} - \frac{\partial \mathcal{L}}{\partial q_i} = 0, \quad (12)$$

where q_i for $i = 1-4$ are order parameters ϵ , φ_1 , β , and ϑ_1 , respectively. As a result, we obtain a system of four coupled differential equations describing the spin dynamics in the magnetoelectric Cr_2O_3

$$\begin{aligned} \dot{\epsilon} + \omega_{\text{A}} \varphi_1 \pm \gamma \beta H_z \pm \tilde{\lambda}_{\text{ME1}} \epsilon E_x - \tilde{\lambda}_{\text{ME1}} \beta E_y \\ - (\tilde{\lambda}_{\text{ME4}} - \tilde{\lambda}_{\text{ME5}}) \beta E_z = \mp \tilde{\lambda}_{\text{SOT}} \dot{E}_y, \end{aligned} \quad (13)$$

$$\begin{aligned} \dot{\varphi}_1 - \omega_{\text{Ex}} \epsilon \pm \gamma \vartheta_1 H_z \mp \tilde{\lambda}_{\text{ME1}} \varphi_1 E_x \\ + \tilde{\lambda}_{\text{ME1}} \vartheta_1 E_y - (\tilde{\lambda}_{\text{ME4}} - \tilde{\lambda}_{\text{ME5}}) \vartheta_1 E_z = \mp \tilde{\lambda}_{\text{ME3}} E_y - \gamma H_y, \end{aligned} \quad (14)$$

$$\begin{aligned} \dot{\beta} + \omega_{\text{A}} \vartheta_1 \mp \gamma \epsilon H_z \mp \tilde{\lambda}_{\text{ME1}} \beta E_x - \tilde{\lambda}_{\text{ME1}} \epsilon E_y \\ + (\tilde{\lambda}_{\text{ME4}} - \tilde{\lambda}_{\text{ME5}}) \epsilon E_z = \tilde{\lambda}_{\text{SOT}} \dot{E}_x, \end{aligned} \quad (15)$$

$$\begin{aligned} \dot{\vartheta}_1 - \omega_{\text{Ex}} \beta \mp \gamma \varphi_1 H_z \pm \tilde{\lambda}_{\text{ME1}} \vartheta_1 E_x + \tilde{\lambda}_{\text{ME1}} \varphi_1 E_y \\ + (\tilde{\lambda}_{\text{ME4}} - \tilde{\lambda}_{\text{ME5}}) \varphi_1 E_z = \tilde{\lambda}_{\text{ME3}} E_x \pm \gamma H_x, \end{aligned} \quad (16)$$

where $\omega_{\text{A}} = \gamma H_{\text{A}} = 2\gamma K/m_0 \simeq 1.2 \times 10^{10} \text{ rad/s}$ [50], $\omega_{\text{Ex}} = \gamma H_{\text{Ex}} = 4\gamma \lambda_{\text{Ex}} m_0 \simeq 8.6 \times 10^{13} \text{ rad/s}$ [50], $\tilde{\lambda}_{\text{ME1-5}} = \gamma \lambda_{\text{ME1-5}}$, $\tilde{\lambda}_{\text{SOT}} = \gamma \lambda_{\text{SOT}} \pi_z \varepsilon / (4\pi)$. The system of differential Eqs. (13)–(16) describes the dynamics of a doubly degenerate magnon in Cr_2O_3 characterized by the frequency $\omega_{\text{M}} = \sqrt{\omega_{\text{Ex}} \omega_{\text{A}}}$, driven by the $\mathbf{E}(t)$ and $\mathbf{H}(t)$ torques appearing on the right-hand side of the equations. Besides, there are intrinsic parametric $\mathbf{E}(t)$ and $\mathbf{H}(t)$ torques on the left side of these

equations, which we neglect for simplicity since they do not significantly affect the effects at the field values of interest. Thus, the system of Eqs. (13)–(16) takes a more straightforward form

$$\dot{\epsilon} + \omega_{\text{A}} \varphi_1 = \mp \tilde{\lambda}_{\text{SOT}} \dot{E}_y, \quad (17)$$

$$\dot{\varphi}_1 - \omega_{\text{Ex}} \epsilon = \mp \tilde{\lambda}_{\text{ME3}} E_y - \gamma H_y, \quad (18)$$

$$\dot{\beta} + \omega_{\text{A}} \vartheta_1 = \tilde{\lambda}_{\text{SOT}} \dot{E}_x, \quad (19)$$

$$\dot{\vartheta}_1 - \omega_{\text{Ex}} \beta = \tilde{\lambda}_{\text{ME3}} E_x \pm \gamma H_x, \quad (20)$$

which can be reduced to four second order differential equations for φ_1 and ϑ_1 describing the dynamics of the magnetization \mathbf{m} and antiferromagnetic vector \mathbf{l} components

$$\ddot{\epsilon} + \omega_{\text{A}} \omega_{\text{Ex}} \epsilon = \mp \tilde{\lambda}_{\text{SOT}} \ddot{E}_y \pm \omega_{\text{A}} \tilde{\lambda}_{\text{ME3}} E_y + \gamma \omega_{\text{A}} H_y, \quad (21)$$

$$\ddot{\varphi}_1 + \omega_{\text{A}} \omega_{\text{Ex}} \varphi_1 = \mp (\omega_{\text{Ex}} \tilde{\lambda}_{\text{SOT}} + \tilde{\lambda}_{\text{ME3}}) \dot{E}_y - \gamma \dot{H}_y, \quad (22)$$

$$\ddot{\beta} + \omega_{\text{A}} \omega_{\text{Ex}} \beta = \tilde{\lambda}_{\text{SOT}} \ddot{E}_x - \omega_{\text{A}} \tilde{\lambda}_{\text{ME3}} E_x \mp \gamma \omega_{\text{A}} H_x, \quad (23)$$

$$\ddot{\vartheta}_1 + \omega_{\text{A}} \omega_{\text{Ex}} \vartheta_1 = (\omega_{\text{Ex}} \tilde{\lambda}_{\text{SOT}} + \tilde{\lambda}_{\text{ME3}}) \dot{E}_x \pm \gamma \dot{H}_x, \quad (24)$$

or using Eq. (32) in the more common form

$$\ddot{m}_x + \omega_{\text{A}} \omega_{\text{Ex}} m_x = \mp \tilde{\lambda}_{\text{SOT}} \ddot{E}_x \pm \omega_{\text{A}} \tilde{\lambda}_{\text{ME3}} E_x + \gamma \omega_{\text{A}} H_x, \quad (25)$$

$$\ddot{m}_y + \omega_{\text{A}} \omega_{\text{Ex}} m_y = \mp \tilde{\lambda}_{\text{SOT}} \ddot{E}_y \pm \omega_{\text{A}} \tilde{\lambda}_{\text{ME3}} E_y + \gamma \omega_{\text{A}} H_y, \quad (26)$$

$$\ddot{l}_x + \omega_{\text{A}} \omega_{\text{Ex}} l_x = (\omega_{\text{Ex}} \tilde{\lambda}_{\text{SOT}} + \tilde{\lambda}_{\text{ME3}}) \dot{E}_y \pm \gamma \dot{H}_y, \quad (27)$$

$$\ddot{l}_y + \omega_{\text{A}} \omega_{\text{Ex}} l_y = -(\omega_{\text{Ex}} \tilde{\lambda}_{\text{SOT}} + \tilde{\lambda}_{\text{ME3}}) \dot{E}_x \mp \gamma \dot{H}_x. \quad (28)$$

As seen from Eqs. (27) and (28), the linear magnetoelectric effect and SOT enter the above equations for dynamics of the antiferromagnetic vector \mathbf{l} in a similar way and have similar dependencies on spin arrangements in different antiferromagnetic domains. If the frequency of the oscillating electric field is much lower than the frequency of the spin resonance, the equations are, however, irrelevant. The NSOT at low frequencies was studied, for instance, in metallic antiferromagnets in Ref. [11]. The metallicity is important because the electric field, being screened by free charge carriers, cannot penetrate into the film, but due to large electric conductivity drives the electric current \mathbf{j} . The oscillating electric field can induce displacement current even in materials with poor electric conductivity and thus also in insulating magnets where

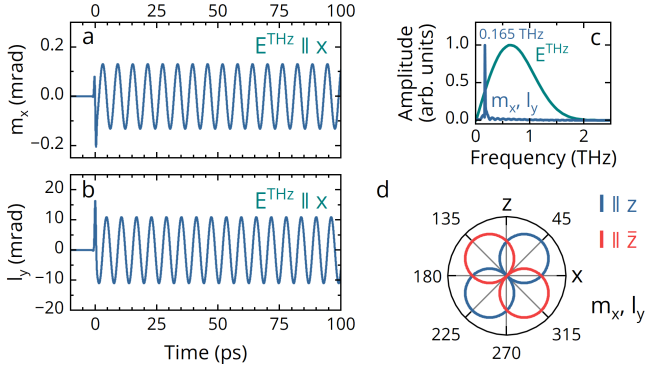


FIG. 3. **Spin dynamics induced by a THz pump pulse in Cr_2O_3 .** Temporal oscillations of (a) magnetization m_x and (b) antiferromagnetic vector l_y components driven by the THz electric field $\mathbf{E}^{\text{THz}} \parallel x$ in a single antiferromagnetic domain. (c) Normalized Fourier spectra of spin dynamics from (a) and (b) compared to the spectrum of the THz pump pulse. (d) Polar diagram of the amplitude of oscillations m_x and l_y as a function of the THz polarization angle for two opposite antiferromagnetic domain with $\mathbf{l} \parallel z$ (blue) and $\mathbf{l} \parallel \bar{z}$ (red).

the screening by free charges is absent and strong electric fields can easily penetrate into the medium. Thus, in addition to the THz magnetoelectric effect reported earlier [10], the SOT is also likely capable of driving the coherent spin dynamics at THz frequencies.

In Ref. [10], it was experimentally demonstrated that a single-cycle THz pump pulse polarized in the plane of the antiferromagnetic vector \mathbf{l} induces spin dynamics of comparable amplitudes, regardless of whether the driving force is the THz electric field ($\mathbf{E}^{\text{THz}} \perp \mathbf{l}$) or the THz magnetic field ($\mathbf{E}^{\text{THz}} \parallel \mathbf{l}$). We performed simulations of this experiment with the THz pump pulse from Fig. 2 polarized in the xz plane, solving Eqs. (25) and (28) with the value $\omega_{\text{Ex}} \tilde{\lambda}_{\text{SOT}} + \tilde{\lambda}_{\text{ME3}} \simeq -1$ which provides equality of amplitudes in both geometries. Figures 3(a) and 3(b) show the transients of m_x and l_y for $\mathbf{E}^{\text{THz}} \parallel x$ in the single antiferromagnetic domain with $\mathbf{l} \parallel z$. The oscillations of m_x and l_y have the frequency of 0.165 THz, corresponding to the antiferromagnetic resonance [50], as confirmed by the Fourier spectra in Fig. 3(c). Notably, the oscillation amplitude depends non-trivially on the polarization angle of \mathbf{E}^{THz} , as shown in Fig. 3(d). This behavior arises from the interference between electric and magnetic field-induced torques, consistent with the experimental findings of Ref. [10]. Interestingly, in an antiferromagnetic domain with the opposite orientation of \mathbf{l} , this angular dependence undergoes a 90° rotation [Fig. 3(d)].

Although the available literature lacks data on the magnitude of the SOT contribution for the insulator Cr_2O_3 , we can estimate it based on known parameters. First, the static magnetoelectric coefficient $\alpha_\perp \simeq -9 \times 10^{-5}$ has been measured in Ref. [24]. This coefficient is related to the magnetoelectric parameter as $\alpha_\perp = \pm \lambda_{\text{ME3}} \chi_\perp$, where χ_\perp is the perpendicular mag-

netic susceptibility [10]. In the static regime, where SOT effects are negligible, these values yield $\lambda_{\text{ME3}} \simeq -0.8$ [24, 50, 51]. Interestingly, optical measurements reveal a magnetoelectric response of comparable magnitude to the static case [52–54]. However, in the THz range, the experimental results, in accordance with Eqs. (27) and (28), do not permit separate determination of the magnetoelectric and SOT contributions. Instead, only their combined effect $\omega_{\text{Ex}} \lambda_{\text{SOT}} \varepsilon / (4\pi) + \lambda_{\text{ME3}} \simeq -1$ is observable. Assuming that the THz magnetoelectric parameter remains close to its static value $\lambda_{\text{ME3}} \simeq -0.8$, we can estimate that the SOT contribution does not exceed $\lambda_{\text{SOT}} / \omega_{\text{Ex}} \lesssim -0.25$.

CONCLUSIONS

In summary, we have discussed an effect analogous to the Néel spin-orbit torque for spin control for the prototype magnetoelectric insulator Cr_2O_3 . Employing symmetry analysis, we reveal a coupling between the antiferromagnetic order parameter and the displacement current induced by the terahertz electric field. Our analysis shows that this coupling should also include the electric dipole order parameter, which stems from the non-zero dipole moments at the Cr^{3+} magnetic ion sites. Using a Lagrangian approach, we derived the equations of spin dynamics, when the considered spin-orbit torque competes with the linear magnetoelectric effect, mirroring behavior observed in metallic antiferromagnets. This indicates that the Néel spin-orbit torque is a more general magnetic phenomenon, not limited to metallic antiferromagnets. Our findings open new avenues for ultrafast spin control in insulating magnetoelectric antiferromagnets by terahertz electric fields, extending beyond the straightforward linear magnetoelectric effect [10] and sum-frequency excitation [55].

METHODS

The sublattice magnetizations in the non-standard spherical coordinate system where the polar angle ϑ counts from the y axis and the azimuthal angle φ lies in the xz plane and counts from the x axis have the form $\mathbf{m}_{\text{A,B}} = (\sin \vartheta_{\text{A,B}} \cos \varphi_{\text{A,B}}, \cos \vartheta_{\text{A,B}}, \sin \vartheta_{\text{A,B}} \sin \varphi_{\text{A,B}})$. Then, the spherical angles of \mathbf{m}_{A} and \mathbf{m}_{B} are parametrized as follows

$$\begin{aligned} \vartheta_{\text{A}} &= \vartheta - \epsilon, & \vartheta_{\text{B}} &= \pi - \vartheta - \epsilon, \\ \varphi_{\text{A}} &= \varphi + \beta, & \varphi_{\text{B}} &= \pi + \varphi - \beta, \end{aligned} \quad (29)$$

where small canting angles $\epsilon \ll 1$ and $\beta \ll 1$ are introduced. This allowed us to expand the net magnetization \mathbf{m} and antiferromagnetic \mathbf{l} vector Cartesian components

in series with respect to ε and β angles

$$\begin{aligned}
m_x &\approx -\beta \sin \vartheta \sin \varphi - \epsilon \cos \vartheta \cos \varphi, \\
m_y &\approx \epsilon \sin \vartheta, \\
m_z &\approx \beta \sin \vartheta \cos \varphi - \epsilon \cos \vartheta \sin \varphi, \\
l_x &\approx \sin \vartheta \cos \varphi, \\
l_y &\approx \cos \vartheta, \\
l_z &\approx \sin \vartheta \sin \varphi.
\end{aligned} \tag{30}$$

The ground state of the antiferromagnetic vector $\mathbf{l} \parallel z$ is defined by the angles $\theta_0 = \frac{\pi}{2}$ and $\varphi_0 = \pm \frac{\pi}{2}$, where \pm denotes two different antiferromagnetic domains. Near the ground state, the angles can be expressed as $\vartheta = \vartheta_0 + \vartheta_1$ and $\varphi = \varphi_0 + \varphi_1$, where $\vartheta_1 \ll 1$ and $\varphi_1 \ll 1$. Then the following expansions are relevant

$$\begin{aligned}
\sin \vartheta &\approx 1 - \frac{\vartheta_1^2}{2}, \quad \cos \vartheta \approx -\vartheta_1, \\
\sin \varphi &\approx \pm \left(1 - \frac{\varphi_1^2}{2}\right), \quad \cos \varphi \approx \mp \varphi_1.
\end{aligned} \tag{31}$$

This allows us to represent Cartesian components of the \mathbf{m} and \mathbf{l} vectors from Eq. (30) in the form

$$\begin{aligned}
m_x &\approx \mp \beta, \\
m_y &\approx \epsilon, \\
m_z &\approx \pm(\epsilon \vartheta_1 - \beta \varphi_1), \\
l_x &\approx \mp \varphi_1, \\
l_y &\approx -\vartheta_1, \\
l_z &\approx \pm \left(1 - \frac{\varphi_1^2}{2} - \frac{\vartheta_1^2}{2}\right).
\end{aligned} \tag{32}$$

DATA AVAILABILITY

No datasets were generated or analyzed during the current study.

ACKNOWLEDGEMENTS

We are grateful to M. A. Frolov for fruitful discussions. R. M. D. acknowledges support of RSF (Grant No. 24-72-00106). A. K. Z. acknowledges support of RSF (Grant No. 22-12-00367). Z. V. G. acknowledges support from the Ministry of Science and Higher Education of Russia (Agreement No. 075-03-2024-123/1). A. V. K. acknowledges support from the European Research Council ERC Grant Agreement No. 101054664 (SPARTACUS).

AUTHOR CONTRIBUTIONS

A. K. Z formulated the idea of the project with inputs from R. M. D. and A. V. K. R. M. D. and A. K. Z. developed and analyzed the theoretical model. Z. V. G. performed the point charge model calculations. All the authors participated in the discussions of the results and gave inputs throughout the project. R. M. D. wrote the manuscript with contributions and comments from all the authors. The project was supervised by A. V. K. and A. K. Z.

COMPETING INTEREST

The authors declare no competing interests and that this work has been published as a result of peer-to-peer scientific collaboration between researchers. The provided affiliations represent the actual addresses of the authors in agreement with their digital identifier (ORCID) and cannot be considered as a formal collaboration between the aforementioned institutions.

-
- [1] J. Han, R. Cheng, L. Liu, H. Ohno, and S. Fukami, Coherent antiferromagnetic spintronics, *Nat. Mater.* **22**, 684 (2023).
 - [2] B. H. Rimmler, B. Pal, and S. S. P. Parkin, Non-collinear antiferromagnetic spintronics, *Nat. Rev. Mater.* **10**, 109 (2025).
 - [3] A. Dal Din, O. Amin, P. Wadley, and K. W. Edmonds, Antiferromagnetic spintronics and beyond, *npj Spintronics* **2**, 25 (2024).
 - [4] H. Yan, X. Zhou, P. Qin, and Z. Liu, Review on spin-split antiferromagnetic spintronics, *Appl. Phys. Lett.* **124**, 10.1063/5.0184580 (2024).
 - [5] V. Baltz, A. Hoffmann, S. Emori, D.-F. Shao, and T. Jungwirth, Emerging materials in antiferromagnetic spintronics, *APL Mater.* **12**, 10.1063/5.0184580 (2024).
 - [6] A. K. Zvezdin, Dynamics of domain walls in weak ferromagnets, *JETP Lett.* **29**, 553 (1979).
 - [7] A. F. Andreev and V. I. Marchenko, Symmetry and the macroscopic dynamics of magnetic materials, *Sov. Phys. Usp.* **130**, 39 (1980).
 - [8] A. K. Zvezdin and A. A. Mukhin, New nonlinear dynamics effects in antiferromagnets, *Bull. Lebedev Phys. Inst.* **12**, 10 (1981).
 - [9] T. Satoh, S.-J. Cho, R. Iida, T. Shimura, K. Kuroda, H. Ueda, Y. Ueda, B. A. Ivanov, F. Nori, and M. Fiebig, Spin Oscillations in Antiferromagnetic NiO Triggered by Circularly Polarized Light, *Phys. Rev. Lett.* **105**, 077402 (2010).
 - [10] V. R. Bilyk, R. M. Dubrovin, A. K. Zvezdin, A. I. Kirilyuk, and A. V. Kimel, Control of spins in collinear an-

- tiferromagnet Cr_2O_3 by terahertz electric fields, *Newton* **1**, 100132 (2025).
- [11] P. Wadley, B. Howells, J. Železný, C. Andrews, V. Hills, R. P. Campion, V. Novák, K. Olejník, F. Maccherozzi, S. Dhesi, *et al.*, Electrical switching of an antiferromagnet, *Science* **351**, 587 (2016).
 - [12] S. Y. Bodnar, L. Šmejkal, I. Turek, T. Jungwirth, O. Gomonay, J. Sinova, A. A. Sapozhnik, H.-J. Elmers, M. Kläui, and M. Jourdan, Writing and reading antiferromagnetic Mn_2Au by Néel spin-orbit torques and large anisotropic magnetoresistance, *Nat. Commun.* **9**, 348 (2018).
 - [13] A. Manchon, J. Železný, I. M. Miron, T. Jungwirth, J. Sinova, A. Thiaville, K. Garello, and P. Gambardella, Current-induced spin-orbit torques in ferromagnetic and antiferromagnetic systems, *Rev. Mod. Phys.* **91**, 035004 (2019).
 - [14] R. E. Troncoso, K. Rode, P. Stamenov, J. M. D. Coey, and A. Brataas, Antiferromagnetic single-layer spin-orbit torque oscillators, *Phys. Rev. B* **99**, 054433 (2019).
 - [15] S. Selzer, L. Salemi, A. Deák, E. Simon, L. Szunyogh, P. M. Oppeneer, and U. Nowak, Current-induced switching of antiferromagnetic order in Mn_2Au from first principles, *Phys. Rev. B* **105**, 174416 (2022).
 - [16] Z. Kašpar, M. Surýnek, J. Zubáč, F. Krizek, V. Novák, R. P. Campion, M. S. Wörnle, P. Gambardella, X. Marti, P. Němec, K. W. Edmonds, S. Reimers, O. J. Amin, F. Maccherozzi, S. S. Dhesi, P. Wadley, J. Wunderlich, K. Olejník, and T. Jungwirth, Quenching of an antiferromagnet into high resistivity states using electrical or ultrashort optical pulses, *Nat. Electron.* **4**, 30 (2021).
 - [17] F. Freimuth, S. Blügel, and Y. Mokrousov, Laser-induced torques in metallic antiferromagnets, *Phys. Rev. B* **103**, 174429 (2021).
 - [18] Y. Behovits, A. L. Chekhov, S. Y. Bodnar, O. Gueckstock, S. Reimers, Y. Lytvynenko, Y. Skourski, M. Wolf, T. S. Seifert, O. Gomonay, M. Kläui, M. Jourdan, and T. Kampfrath, Terahertz néel spin-orbit torques drive nonlinear magnon dynamics in antiferromagnetic Mn_2Au , *Nat. Commun.* **14**, 6038 (2023).
 - [19] J. L. Ross, P.-I. Gavriloaea, F. Freimuth, T. Adamantopoulos, Y. Mokrousov, R. F. Evans, R. Chantrell, R. M. Otxoa, and O. Chubykalo-Fesenko, Ultrafast antiferromagnetic switching of Mn_2Au with laser-induced optical torques, *npj Comput. Mater.* **10**, 234 (2024).
 - [20] K. Olejník, Z. Kašpar, J. Zubáč, S. Telkamp, A. Farkaš, D. Kriegner, K. Vybourný, J. Železný, Z. Šobán, P. Zeng, *et al.*, Quench switching of Mn_2As , arXiv preprint arXiv:2411.01930 [10.48550/arXiv.2411.01930](https://arxiv.org/abs/2411.01930) (2024).
 - [21] F. Thöle, A. Keliri, and N. A. Spaldin, Concepts from the linear magnetoelectric effect that might be useful for antiferromagnetic spintronics, *J. Appl. Phys.* **127**, 10.1063/5.0006071 (2020).
 - [22] I. E. Dzyaloshinskii, On the magneto-electrical effects in antiferromagnets, *Sov. Phys. JETP* **10**, 628 (1960).
 - [23] D. N. Astrov, The magnetoelectric effect in antiferromagnets, *Sov. Phys. JETP* **11**, 708 (1960).
 - [24] D. N. Astrov, Magnetoelectric effect in chromium oxide, *Sov. Phys. JETP* **13**, 729 (1961).
 - [25] G. T. Rado and V. J. Folen, Observation of the Magnetically Induced Magnetoelectric Effect and Evidence for Antiferromagnetic Domains, *Phys. Rev. Lett.* **7**, 310 (1961).
 - [26] J. Volger, Anomalous specific heat of chromium oxide (Cr_2O_3) at the antiferromagnetic Curie temperature, *Nature* **170**, 1027 (1952).
 - [27] T. R. McGuire, E. J. Scott, and F. H. Grannis, Antiferromagnetism in a Cr_2O_3 Crystal, *Phys. Rev.* **102**, 1000 (1956).
 - [28] B. N. Brockhouse, Antiferromagnetic structure in Cr_2O_3 , *J. Chem. Phys.* **21**, 961 (1953).
 - [29] L. M. Corliss, J. M. Hastings, R. Nathans, and G. Shirane, Magnetic structure of Cr_2O_3 , *J. Appl. Phys.* **36**, 1099 (1965).
 - [30] E. Bousquet, E. Lelièvre-Berna, N. Qureshi, J.-R. Soh, N. A. Spaldin, A. Urru, X. H. Verbeek, and S. F. Weber, On the sign of the linear magnetoelectric coefficient in Cr_2O_3 , *J. Phys. Condens. Matter* **36**, 155701 (2024).
 - [31] Z. V. Gabbasova, M. D. Kuz'min, A. K. Zvezdin, I. S. Dubenko, V. A. Murashov, D. N. Rakov, and I. B. Krynetsky, $\text{Bi}_{1-x}\text{R}_x\text{FeO}_3$ (R = rare earth): a family of novel magnetoelectrics, *Phys. Lett. A* **158**, 491 (1991).
 - [32] C. Ederer and N. A. Spaldin, Influence of strain and oxygen vacancies on the magnetoelectric properties of multiferroic bismuth ferrite, *Phys. Rev. B* **71**, 224103 (2005).
 - [33] A. K. Zvezdin, Z. V. Gareeva, and X. M. Chen, Multiferroic order parameters in rhombic antiferromagnets RCrO_3 , *J. Phys. Condens. Matter* **33**, 385801 (2021).
 - [34] R. Resta and D. Vanderbilt, Theory of polarization: a modern approach, in *Physics of ferroelectrics: a modern perspective* (Springer, 2007) pp. 31–68.
 - [35] C. Kittel, Theory of antiferroelectric crystals, *Phys. Rev.* **82**, 729 (1951).
 - [36] A. K. Tagantsev, K. Vaideeswaran, S. B. Vakhrušev, A. V. Filimonov, R. G. Burkovsky, A. Shaganov, D. Andronikova, A. I. Rudskoy, A. Q. R. Baron, H. Uchiyama, D. Chernyshov, A. Bosak, Z. Ujma, K. Roleder, A. Majchrowski, J.-H. Ko, and N. Setter, The origin of antiferroelectricity in PbZrO_3 , *Nat. Commun.* **4**, 2229 (2013).
 - [37] E. A. Turov, A. V. Kolchanov, V. V. Menshenin, I. F. Mirsaev, and V. V. Nikolaev, Symmetry and Physical Properties of Antiferromagnets, Fizmatlit, Moscow (2001).
 - [38] E. A. Turov and V. V. Nikolaev, New physical phenomena caused by magnetoelectric and antiferroelectric interactions in magnets, *Phys.-Usp.* **48**, 431 (2005).
 - [39] A. Manchon, H. C. Koo, J. Nitta, S. M. Frolov, and R. A. Duine, New perspectives for rashba spin-orbit coupling, *Nat. Mater.* **14**, 871 (2015).
 - [40] J. Železný, H. Gao, A. Manchon, F. Freimuth, Y. Mokrousov, J. Zemen, J. Mašek, J. Sinova, and T. Jungwirth, Spin-orbit torques in locally and globally noncentrosymmetric crystals: Antiferromagnets and ferromagnets, *Phys. Rev. B* **95**, 014403 (2017).
 - [41] L. Salemi, M. Berritta, A. K. Nandy, and P. M. Oppeneer, Orbitaly dominated rashba-edelstein effect in noncentrosymmetric antiferromagnets, *Nat. Commun.* **10**, 5381 (2019).
 - [42] G. Bihlmayer, P. Noël, D. V. Vyalikh, E. V. Chulkov, and A. Manchon, Rashba-like physics in condensed matter, *Nat. Rev. Phys.* **4**, 642 (2022).
 - [43] A. K. Zvezdin, A. V. Kimel, D. I. Plokhov, and K. A. Zvezdin, Ultrafast spin dynamics in the iron borate easy-plane weak ferromagnet, *J. Exp. Theor. Phys.* **131**, 130 (2020).
 - [44] L. Landau and E. Lifshitz, *Electrodynamics of continuous media*, Vol. 8 (Pergamon, 1984).

- [45] D. V. Sivukhin, *A Course of General Physics. Vol. III, Electricity* (Nauka, Moscow (in Russian), 1996).
- [46] O. D. Jefimenko, *Electricity and magnetism: An introduction to the theory of electric and magnetic fields* (Appleton-Century-Crofts, 1966).
- [47] G. Lucovsky, R. J. Sladek, and J. W. Allen, Infrared-active phonons in Cr_2O_3 , *Phys. Rev. B* **16**, 4716 (1977).
- [48] E. Fradkin, *Field theories of condensed matter physics* (Cambridge University Press, 2013).
- [49] A. K. Zvezdin, R. M. Dubrovin, and A. V. Kimel, Giant Parametric Amplification of the Inverse Cotton–Mouton Effect in Antiferromagnetic Crystals, *JETP Lett.* **119**, 363 (2024).
- [50] S. Foner, High-Field Antiferromagnetic Resonance in Cr_2O_3 , *Phys. Rev.* **130**, 183 (1963).
- [51] A. A. Mukhin, V. D. Travkin, and S. P. Lebedev, BWO quasi-optical spectroscopy of Cr_2O_3 : Gyrotropic birefringence at antiferromagnetic resonance, *Ferroelectrics* **204**, 261 (1997).
- [52] R. V. Pisarev, B. B. Krichevtsov, and V. V. Pavlov, Optical study of the antiferromagnetic-paramagnetic phase transition in chromium oxide Cr_2O_3 , *Phase Transitions* **37**, 63 (1991).
- [53] B. B. Krichevtsov, V. V. Pavlov, R. V. Pisarev, and V. N. Gridnev, Spontaneous non-reciprocal reflection of light from antiferromagnetic Cr_2O_3 , *J. Phys. Condens. Matter* **5**, 8233 (1993).
- [54] B. B. Krichevtsov, V. V. Pavlov, R. V. Pisarev, and V. N. Gridnev, Magnetoelectric Spectroscopy of Electronic Transitions in Antiferromagnetic Cr_2O_3 , *Phys. Rev. Lett.* **76**, 4628 (1996).
- [55] D. M. Juraschek, D. S. Wang, and P. Narang, Sum-frequency excitation of coherent magnons, *Phys. Rev. B* **103**, 094407 (2021).